논문

A Shock Stable Roe Scheme

Sung-soo Kim[*1], Chongam Kim[*2], Oh-Hyun Rho[*3] and Seung Kyu Hong[*4]

충격파 불안정성을 제거한 Roe 수치기법

김성수[*1], 김종암[*2], 노오현[*3], 홍승규[*4]

본 논문은 충격파 불안정성이 나타나지 않는 충격파 안정적인 수치기법의 개발을 목표로 하고 있다. Roe의 수치기법은 유동의 수치계산에 있어 높은 정확도를 보장하지만 carbuncle 현상과 같은 충격파 불안정성이 나타나는 것으로 알려져 있다. Roe의 수치기법과 HLLE 수치기법의 수치점성을 비교하여 충격파 불안정성의 원인을 살펴보았으며, Roe의 수치기법에 나타나는 반감쇠항에 마하수의 함수인 조절함수 f와 g를 도입하여 충격파 안정성을 획득하였다. 본 논문에서 제안된 수치기법을 다양한 유동문제에 적용하여 수치기법의 충격파 안정성과 정확성을 검증하였다.

Key words: shock instability, accuracy, robustness, Roe's FDS, HLLE, RoeM

1. Introduction

It is essential that a numerical representation of inviscid fluxes, namely the numerical flux function, guarantees the properties of accuracy and robustness in computational fluid dynamics (CFD). The Flux Difference Splitting (FDS) scheme is one of the most successful groups among the various schemes, and is widely used and studied. The FDS schemes follow the idea of Godunov [1] and utilizes the Riemann problem locally. Roe's FDS [2], Osher's one [3] and HLLEM [4] are classified into this family. These FDS schemes can capture contact discontinuity and give good resolution for the boundary layer in viscous flow calculation.

* 2001년 9월 25일 접수

*1 Ph. D. Candidate, Department of Aerospace Engineering, Seoul National University

*2 Assistant Professor, Department of Aerospace Engineering, Seoul National University, Corresponding Author.

*3 Professor, Department of Aerospace Engineering, Seoul National University

*4 Senior Researcher, Agency for Defense Development, Taejeon, Korea

Despite these properties and the good shock capturing property, some disastrous failing is also found in certain problems. This pathological behavior, named 'carbuncle phenomenon', was first observed by Peery and Imlay [5] for blunt body computation with Roe's FDS. The carbuncle phenomenon consists of a protuberant shock profile obtained when a supersonic flow is calculated over a blunt body. The attempts to cure the shock instability can be categorized into two groups. One is to use an entropy fix and the other to use a dissipative counterpart scheme.

Quirk [6] noticed that some schemes that have the property of good capture of contact discontinuity show the shock instability, and some schemes that are free from the shock instability do not capture contact discontinuity. Thus, he suggests that in shock region, a dissipative scheme (HLLE) should be used while a less-dissipative scheme (Roe's FDS) should be used elsewhere. In order to flag the cell interface where the dissipative scheme is needed, a sensor based on pressure gradient is used. Wada and Liou [7], by the same philosophy, suggest this flagging procedure but they used a sonic point

for the flag. For a less-dissipative scheme AUSMDV is used, and for a dissipative scheme, Hänel FVS is adopted. This cure is very efficient, as demonstrated by the results reported in [6,7]. However, this kind of approach always needs a counterpart that stabilizes the original flux function, and the selection itself is a critical problem. An inadequate counterpart may easily compromise the accuracy of the numerical solution, especially in the case of hypersonic flow.

An entropy fix to the linear field is to limit the minimum value of the wave speed, and consequently adds numerical dissipation to damp out spurious oscillation. Peery and Imlay [5] proposed an anisotropic function for the entropy fix, and Lin [8] proposed an isotropic correction function using a pressure gradient sensor. This entropy fix successfully cured the shock instability. However, this achievement critically depended on where and how much dissipation was added. Improper entropy fix may broaden the shock wave profile and/or deteriorate the boundary layer resolution. These two methods are the same in the sense that dissipation is added to the original scheme, and both need the detecting procedure to flag the cell interface where a tuning parameter usually appears.

So far, it is believed that the scheme that captures contact discontinuity, *i.e.,* that has vanishing dissipation in stationary contact discontinuity, cannot avoid the shock instability and the only way to prevent the shock instability is to add enough dissipation to damp out oscillation. However, Liou [9] observed that all the tested numerical flux functions that suffered from the shock instability have a term depending on pressure difference in the mass flux, and those that are free from the shock instability are independent of pressure difference in the mass flux, finally reaching the following conjecture, '*The condition* $D^p \neq 0, \forall M$ *, in the mass flux is necessary for a scheme to develop, as t increases, the shock instability as manifested by the odd-even decoupling and carbuncle phenomenon. On the other hand, the condition* $D^p = 0, \forall M$ *is sufficient for a scheme to prevent the shock instability from occurring.*' This analysis shows that it is possible to devise a flux function free from the shock instability, with vanishing dissipation in capturing contact discontinuity.

The present study aims at the design of a new flux scheme that is free from the shock instability. We select Roe's FDS as the basic scheme. Following Liou's conjecture, we focus on the treatment of the pressure term in the mass flux.

The paper is organized as follows. As a brief review, numerical examples with the shock instability are presented in Section 1. In Section 2, we present the modification procedure of Roe's flux function and propose Roe with Mach number-based function (RoeM) schemes. In Section 3, we present the numerical results and discuss the properties of the schemes proposed in Section 2. Finally, concluding remarks are given.

2. Shock Instability

1.1 Quirk's test

In order to judge whether a scheme is shock stable or not, Quirk [6] presents a simplified test case named 'odd-even decoupling', a planar moving shock in a duct where a centerline grid is perturbed. The computational mesh has a nominally uniform grid of 20×800 cells with unit spacing, the centerline of which is perturbed from that of a perfectly uniform mesh in the following manner:

$$Y_{i,j,mid} = \begin{cases} Y_{j,mid} + 10^{-4}, & \text{for } j \text{ even} \\ Y_{j,mid} - 10^{-4}, & \text{for } j \text{ odd} \end{cases}$$

The shock wave is traveling with a Mach number $M_s = 6.0$. For this calculation, Roe's FDS is used. The result is presented in Fig. 1, which shows density contour after 300 iterations with the CFL number of 0.5. As the shock propagates downstream, perturbation grows from the center where the grid is perturbed, and eventually the planar shock breaks down.

1.2 Double Mach reflection

Another the shock instability behavior is observed when a plane shock wave is reflected from a ramp in the Double-Mach Reflection (DMR) regime. The principal Mach stem is so severely kinked that an unphysical triple point appears. This pathological

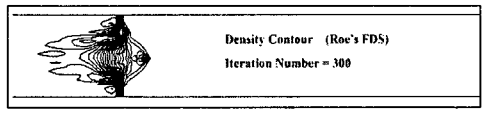

Fig. 1 Quirk's test

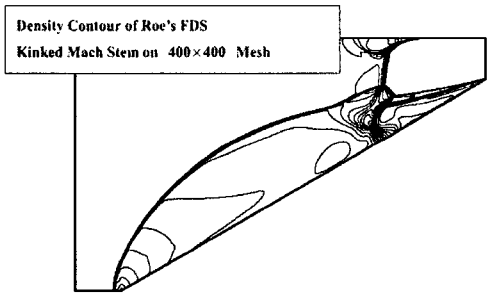

Fig. 2 Kinked Mach stem

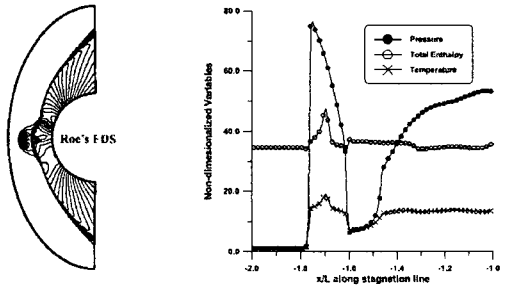

Fig. 3 Carbuncle phenomenon

behavior is named the kinked Mach stem. This test consists of a 30° ramp and a moving shock with $M_s=5.5$. In Fig. 2, density contour of Roe's FDS on a 400×400 mesh is shown. The incident shock wave breaks down and the Mach stem protrudes like a beak at the wall.

1.3 The carbuncle phenomenon

The carbuncle phenomenon was first reported by Peery and Imlay [5] for blunt body flow computation. We include in Fig. 3 pressure contour and shock profiles along the stagnation line of a half cylinder. The free stream Mach number is 8.0, the mesh size is 65×113 and Roe's FDS is used in the first-order accuracy. Figure 3 shows the unsymmetrical behavior and protuberance of bow shock.

2. Improved Roe Scheme

2.1 Roe's flux function

The governing equations of inviscid flow in two-dimension are as follows:

$$\frac{\partial Q}{\partial t}+\frac{\partial E}{\partial x}+\frac{\partial G}{\partial y}=0, \tag{1}$$

where the state vector and flux vectors are

$$Q=\begin{pmatrix}\rho\\ \rho u\\ \rho v\\ \rho e_t\end{pmatrix}, E=\begin{pmatrix}\rho u\\ \rho u^2+p\\ \rho uv\\ \rho uH\end{pmatrix}, G=\begin{pmatrix}\rho v\\ \rho uv\\ \rho v^2+p\\ \rho vH\end{pmatrix} \tag{2}$$

The equation of state has the form as follows:

$$p=(\gamma-1)\rho e=(\gamma-1)\rho\left[e_t-\frac{1}{2}(u^2+v^2)\right], \tag{3}$$

where γ is the specific heat ratio and has the value of 1.4 for a perfect gas.

The numerical flux of Roe's FDS [2] at the cell interface is written as follows:

$$F_{j+\frac{1}{2}}=\frac{1}{2}[F_j+F_{j+1}-|\hat{A}|\Delta Q] \tag{4}$$

In order to make analysis easier, we rearrange the flux function of Roe's FDS in another form in the subsonic region as follows:

$$F_{j+\frac{1}{2}}=\frac{1}{2}[F_j+F_{j+1}-\hat{M}(F_{j+1}-F_j)+\hat{c}(\hat{M}^2-1)\Delta Q+\hat{c}(1-|\hat{M}|)B\Delta Q] \quad (5a)$$

$$B\Delta Q=\left(\Delta p-\frac{\Delta p}{\hat{c}^2}\right)\begin{pmatrix}1\\ \hat{u}\\ \hat{v}\\ \frac{\hat{u}^2+\hat{v}^2}{2}\end{pmatrix}+\hat{\rho}\begin{pmatrix}0\\ \Delta u-n_x\Delta U\\ \Delta v-n_y\Delta U\\ \hat{u}\Delta u+\hat{v}\Delta v-\hat{U}\Delta U\end{pmatrix} \quad (5b)$$

U indicates contravariant velocity and n_x, n_y are unit normal vector components at the cell interface. $\hat{}$ indicates Roe-averaged values at the cell interface. In the above expression, Δp exists only in the last term $B\Delta Q$, which is a kind of anti-diffusion term that enables Roe's FDS to capture contact discontinuity exactly and is thought to trigger the shock instability. This will become obvious when Roe's FDS is compared with HLLE scheme.

2.2 Cure for the shock instability

It is well known that HLLE scheme cannot capture contact discontinuity but is free from the shock instability. The numerical flux of HLLE is written as follows:

$$F_{j+\frac{1}{2}}=\frac{1}{2}[F_j+F_{j+1}-\hat{M}(F_{j+1}-F_j)+\hat{c}(\hat{M}^2-1)\Delta Q] \quad (6)$$

where Roe-averaged values are used for the non-linear wave speeds. Equation (6) is identical to Eq. (5) except the last term $B\Delta Q$ in Eq. (5). As mentioned before, $B\Delta Q$ enables Roe's FDS to capture contact discontinuity and triggers the shock instability.

In the present paper, it is suggested that the dissipation coefficient depending on pressure difference in continuity equation, D^p, is modified as the following in order to control density fluctuation in the mass flux:

$$\frac{D^p}{\hat{c}^2}=\hat{c}f(1-|\hat{M}|),\quad f=\begin{cases}1 & \hat{u}^2+\hat{v}^2=0\\ |\hat{M}|^h & elsewhere\end{cases} \quad (7a)$$

$$h=1-\min(P_{i,j+\frac{1}{2}},P_{i-\frac{1}{2},j},P_{i+\frac{1}{2},j},P_{i-\frac{1}{2},j+1},P_{i+\frac{1}{2},j+1}) \quad (7b)$$

$$P_{i,j+\frac{1}{2}}=\min\left(\frac{p_{i,j}}{p_{i,j+1}},\frac{p_{i,j+1}}{p_{i,j}}\right) \quad (7c)$$

Figure 4 shows the dissipative coefficients in the case where h has the value of unity. The function f and D^p will become zero when the cell interface Mach number is zero. It is noted that the dissipation coefficient of pressure is balanced with that of density.

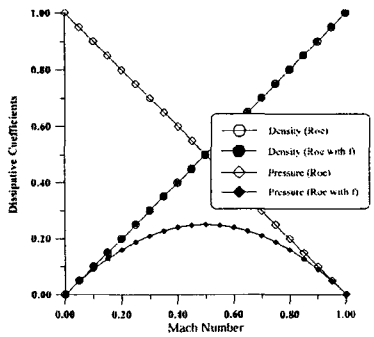

Fig. 4 Dissipative coefficients

Considering the odd-even decoupling problem defined in [6], we can examine how Roe's FDS with the function f evolves the sawtooth-type data. We assume that the 2-D computational mesh is uniform and the discrete solution at time t^n is given by

$$\rho_j^n=\rho+\tilde{\rho}^n,\ p_j^n=p+\tilde{p}^n,\ u_j^n=u^0,\ v_j^n=v^0 \quad (8a)$$

if j is even and by

$$\rho_j^n=\rho-\tilde{\rho}^n,\ p_j^n=p-\tilde{p}^n,\ u_j^n=u^0,\ v_j^n=v^0 \quad (8b)$$

if j is odd. Here, $\tilde{\rho}^n$ and $\tilde{p}^n$ are the amplitudes of the sawtooth profiles for the

density and pressure fields respectively. For Roe's FDS with the function f, the amplitude at the $n+1$ time level can be manipulated to give

$$\tilde{\rho}^{n+1} = (1-2\nu_y|M|)\,\tilde{\rho}^n - \frac{2\nu_y}{c^2}(1-|M|)|M|^h\,\tilde{p}^n \quad (9a)$$

$$\tilde{p}^{n+1} = [1-2\nu_y|M|^h\{1+(\gamma-1)M^2\}]\,\tilde{p}^n \quad (9b)$$

where $\nu_y = \frac{c\Delta t}{\Delta y}$, $M = \frac{v}{c}$. When cell interface velocity is not zero, pressure and density are stable, i.e. density perturbation and pressure perturbation decay as time goes on. When cell interface velocity is zero, pressure and density are neutrally stable, i.e. no growth and no decay. However, if pressure difference exists, it will drive convective flow, and velocity across the cell interface will have the role of damping out perturbed property. The rate at which density perturbation is damped out is equal to the dissipation coefficient of density, and the rate at which the pressure field feeds density perturbation is equal to the dissipation coefficient of pressure, decreasing as pressure perturbation increases. Liou's conjecture and the above analysis show that the importance is the relation between the feeding rate and the damping rate in density perturbation. Certainly, if the pressure field is continuously perturbed and the damping rate in Eq. (9) is not sufficient, then the function f may be ineffective especially in unsteady flow computation, and rigorous non-linear analysis concerning dynamic behavior of flow property may be required. However, in most numerical tests performed in this paper, the function f seems to be sufficient to prevent the shock instability from occurring. The numerical flux of Roe's FDS with the function f defined in Eq. (7) is given by

$$F_{j+\frac{1}{2}} = \frac{b_1\times F_j - b_2\times F_{j+1}}{b_1-b_2} + \frac{b_1\times b_2}{b_1-b_2}\Delta Q - \frac{b_1\times b_2}{b_1-b_2}\times\frac{1}{1+|\hat{M}|}B\Delta Q \quad (10a)$$

$$B\Delta Q = \left(\Delta p - f\frac{\Delta p}{\hat{c}^2}\right)\begin{pmatrix}1\\ \hat{u}\\ \hat{v}\\ \frac{\hat{u}^2+\hat{v}^2}{2}\end{pmatrix} + \hat{\rho}\begin{pmatrix}0\\ \Delta u - n_x\Delta U\\ \Delta v - n_y\Delta U\\ \hat{u}\Delta u + \hat{v}\Delta v - \hat{U}\Delta U\end{pmatrix} \quad (10b)$$

$$b_1 = \max(0, \hat{U}+\hat{c}),\quad b_2 = \min(0, \hat{U}-\hat{c}) \quad (10c)$$

Equation (10) has the same form as HLLE except $B\Delta Q$ and the definitions of b_1 and b_2.

The case, which shows that the function f is not sufficient to prevent the shock instability, is a double Mach reflection problem. AUSM+ shows an unphysical triple point [10] even though it has the property $D^p = 0,\ \forall M$. In this case, the damping rate in Eq. (9) is thought to be slow compared with the rate at which pressure perturbation is generated from the computational mesh. We think that this phenomenon is due to the unsteadiness of the flow. In order to cure this situation, i.e. to increase the damping rate, function g is introduced as follows:

$$F_{j+\frac{1}{2}} = \frac{b_1\times F_j - b_2\times F_{j+1}}{b_1-b_2} + \frac{b_1\times b_2}{b_1-b_2}\Delta Q - g\frac{b_1\times b_2}{b_1-b_2}\times\frac{1}{1+|\hat{M}|}B\Delta Q \quad (11a)$$

$$g = \begin{cases} |M|^{1-\min\left(\frac{p_j}{p_{j+1}}, \frac{p_{j+1}}{p_j}\right)}, & M\neq 0 \\ 1, & M = 0 \end{cases} \quad (11b)$$

2.3 Total enthalpy conservation

Roe's FDS does not preserve the total enthalpy in inviscid steady flow. The dissipation of the continuity equation and the energy equation in the subsonic region is given by

$$\begin{bmatrix} D_{continuity} \\ D_{energy} \end{bmatrix} = \hat{c}\Delta\rho|\hat{M}|\begin{bmatrix} 1 \\ H \end{bmatrix} + f\frac{1-|\hat{M}|}{\hat{c}}\Delta p\begin{bmatrix} 1 \\ H \end{bmatrix} + \hat{\rho}\hat{M}\Delta U\begin{bmatrix} 1 \\ H \end{bmatrix} + \hat{\rho}\hat{c}|\hat{M}|\begin{bmatrix} 0 \\ \Delta H \end{bmatrix} + f\Delta p\begin{bmatrix} 0 \\ \hat{U}\hat{M}-\hat{c}|\hat{M}| \end{bmatrix} - \Delta U\begin{bmatrix} 0 \\ \hat{c}^2\hat{\rho}(|\hat{M}|-1)\hat{M} \end{bmatrix} \quad (12)$$

In order for the numerical flux to preserve the total enthalpy, the following condition should be satisfied:

$$D_{energy} = D_{continuity} \times H \quad (13)$$

Equation (12) shows that the last two terms are the error sources. Now, the total enthalpy conservation property is easily obtained just by removing the last two terms. Then, the modified Roe scheme with the total enthalpy conservation property has an expression written by

$$F_{j+\frac{1}{2}} = \frac{b_1 \times F_j - b_2 \times F_{j+1}}{b_1 - b_2} + \frac{b_1 \times b_2}{b_1 - b_2}\Delta Q^* - \frac{b_1 \times b_2}{b_1 - b_2} \times \frac{1}{1+|\hat{M}|} B^*\Delta Q \quad (14a)$$

$$\Delta Q^* = \Delta\begin{pmatrix} \rho \\ \rho u \\ \rho v \\ \rho H \end{pmatrix}, B^*\Delta Q = \left(\Delta\rho - f\frac{\Delta p}{\hat{c}^2}\right)\begin{pmatrix} 1 \\ \hat{u} \\ \hat{v} \\ \hat{H} \end{pmatrix} + \hat{\rho}\begin{pmatrix} 0 \\ \Delta u - n_x\Delta U \\ \Delta v - n_y\Delta U \\ \Delta H \end{pmatrix} \quad (14b)$$

$$b_1 = \max(0, \hat{U}+\hat{c}), \quad b_2 = \min(0, \hat{U}-\hat{c}) \quad (14c)$$

2.4 Expansion shock, instability in the expansion region

Another failing of Roe's FDS is the appearance of expansion shock. Roe's FDS cannot distinguish the expansion shock from the compression shock. Also, in a highly energetic flow, Roe's FDS often calculates physically unacceptable values, negative density and negative temperature, this concerns the positivity condition. Einfeldt et al. [4] showed that no Godunov-type scheme based on a linearized Riemann solution is positively conservative, and they concluded that the reason for the failure of Roe's FDS is that the numerical signal velocities of Roe's Riemann solver underestimates the physical signal velocities. Einfeldt et al. considered not only the numerical signal velocities at a cell interface, but also the numerical signal velocities at neighboring cells and re-defined the eigenvalues of the dissipation matrix. Using these re-defined eigenvalues, Eq. (14) can be re-formulated as follows.

$$F_{j+\frac{1}{2}} = \frac{b_1 \times F_j - b_2 \times F_{j+1}}{b_1 - b_2} + \frac{b_1 \times b_2}{b_1 - b_2}\Delta Q^* - \frac{b_1 \times b_2}{b_1 - b_2} \times \frac{1}{1+|\hat{M}|} B\Delta Q \quad (15a)$$

$$b_1 = \max(0, \hat{U}+\hat{c}, U_{i+1}+c_{i+1}), b_2 = \min(0, \hat{U}-\hat{c}, U_i - c_i) \quad (15b)$$

2.5 Contact discontinuity

In order to resolve the boundary layer accurately in viscous flow, it is essential to capture contact discontinuity. The exact solution for contact discontinuity moving with speed u_c requires that

$$F^{continuity}_{j+\frac{1}{2}} = \frac{1}{2}[\rho_j u_j + \rho_{j+1}u_{j+1} - |u_c|\Delta\rho] \quad (16)$$

After some manipulations, the dissipative coefficient of Eq. (15) is obtained as follows. For $u_j = u_{j+1} = u_c$, $p_j = p_{j+1} = \hat{p}$, and $\rho_j \neq \rho_{j+1}$

$$D^p = \left|\frac{u_c}{(\alpha+\beta)(\hat{c}+u_c)}(2\hat{c}u_c + \alpha\hat{c} - \alpha u_c - \beta\hat{c} + \beta u_c + 2\alpha\beta)\right| \quad (17a)$$

$$b_1 = u_c + \alpha, \; b_2 = u_c - \beta \; (0 \le u_c \le \hat{c}) \quad (17b)$$

For moving contact discontinuity with $\rho_j > \rho_{j+1}$

$$u_c \neq 0, \; \alpha \neq \hat{c}, \; \beta = \hat{c} \quad (18a)$$

$$\left|\frac{u_c}{(a+\hat{c})(\hat{c}+u_c)}(3\hat{c}u_c+3a\hat{c}-au_c-\hat{c}^2)\right|\neq|u_c| \quad (18b)$$

The above expressions show that under certain conditions, the re-formulated scheme in Eq. (15) cannot capture contact discontinuity exactly. Just introducing the concept of the common speed of sound can easily cure it.

RoeM 1 (Roe scheme with Mach number-based function 1)

$$F_{j+\frac{1}{2}}=\frac{b_1\times F_j-b_2\times F_{j+1}}{b_1-b_2}+\frac{b_1\times b_2}{b_1-b_2}\Delta Q^* -\frac{b_1\times b_2}{b_1-b_2}\times\frac{1}{1+|\hat{M}|}B^*\Delta Q \quad (19a)$$

$$b_1=\max(0,\hat{U}+\hat{c},U_{j+1}+\hat{c}),b_2=\min(0,\hat{U}-\hat{c},U_j-\hat{c}) \quad (19b)$$

RoeM 2

$$F_{j+\frac{1}{2}}=\frac{b_1\times F_j-b_2\times F_{j+1}}{b_1-b_2}+\frac{b_1\times b_2}{b_1-b_2}\Delta Q^* -g\frac{b_1\times b_2}{b_1-b_2}\times\frac{1}{1+|\hat{M}|}B^*\Delta Q \quad (20)$$

Now, RoeM 1 and RoeM 2 with the common speed of sound in signal velocities satisfy Eq. (16), still providing sufficient numerical dissipation in the expansion region to prevent an expansion shock.

For $u_j=u_{j+1}=u_{c,p}=p_{j+1}=\hat{p}$, and $\rho_j\neq\rho_{j+1}$

$$D^{\rho}_{RoeM1,2}=|u_c| \quad (21)$$

1-D shock tube test and contact discontinuity problems are solved to confirm the above analysis of the RoeM schemes and results are compared with those of Roe's FDS. This 1-D shock tube case is similar to the classical Sod test, but with special initial conditions given as $\rho_l=3, u_l=0.9, p_l=3$ and $\rho_r=1, u_l=0.9, p_r=1$, with a sonic point along the rarefaction wave. Roe's FDS has an entropy violating solution, an expansion shock as shown in Fig. 5. RoeM 1 and RoeM 2 add dissipation in the expansion region and prevent the formation of an expansion shock. Results of a slowly moving contact discontinuity are shown in Fig. 6. The initial conditions are $\rho_l=10.0, u_l=0.1125, p_l=1$ and $\rho_r=0.125, u_r=0.1125, p_r=1$. The iteration count is 500 with a CFL number of 0.85, and the grid points are 100. This condition corresponds to case 3. As mentioned before, both RoeM 1 and RoeM 2 satisfy Eq. (16) and give accurate results, identical to that from Roe's FDS.

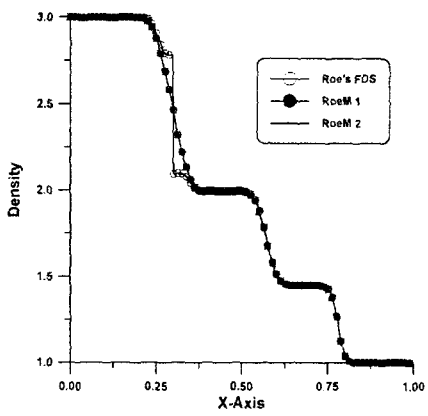

Fig. 5 Sod test with sonic point

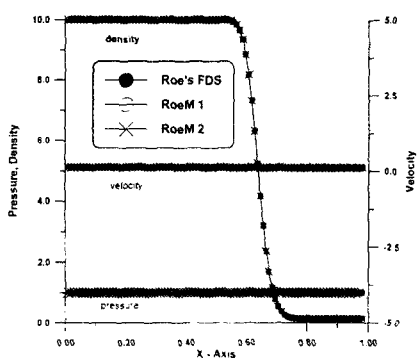

Fig. 6. Slowly moving contact discontinuity

3. Numerical Results

In this section, we demonstrate the capabilities of the proposed schemes with carefully selected test cases.

3.1 Shock instability

Supersonic Flow around a Half-Cylinder. The carbuncle phenomenon around a blunt body is illustrated in Section 1.3. RoeM 1 and RoeM 2 are used to calculate a supersonic inviscid flow around a half-cylinder. This problem has the same initial condition and mesh as the test case in Section 1.3. Figure 7 shows pressure contour and shock profiles which show monotonic behavior. There is no symptom of the carbuncle phenomenon.

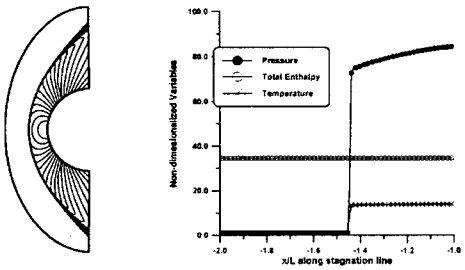

(a) RoeM 1

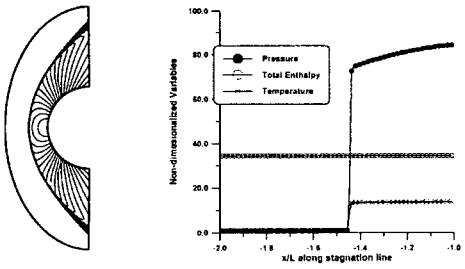

(b) RoeM 2

Fig. 7 Pressure contour and shock profiles

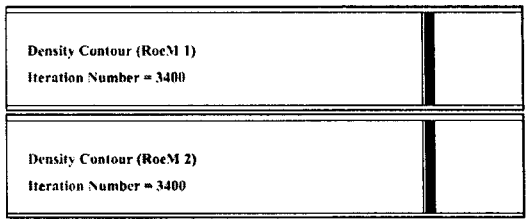

Fig. 8 Quirk's test

Figure 7 also shows the preservation of total enthalpy, which is essential in predicting heat flux accurately at the wall.

Quirk's Test (Odd-Even Decoupling). The description of this test is described in Section 1.1. Roe's FDS amplifies the initial perturbation and completely destroys the normal shock as shown in Fig. 1. Figure 8 shows density contour after 3400 iterations. All of the presented schemes, RoeM 1 and RoeM 2 clearly capture the shock, and initial perturbations do not seem to grow with time.

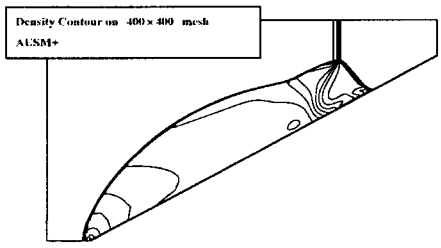

(a) AUSM+

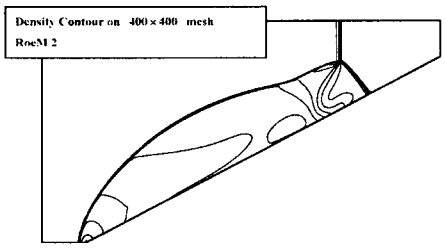

(b) RoeM 2

Fig. 9 Double Mach reflection

The Kinked Mach Stem. In Section 1.2, we showed that Roe's FDS suffers from the kinked Mach stem. Gressier et al. [10] showed that even the AUSM+ scheme on a refined mesh can suffer from the kinked Mach stem. Density contour of AUSM+ and RoeM 2 on a 400×400 mesh are shown in Fig. 9. The kink is about to develop in the AUSM+ scheme in the principal Mach stem, while RoeM 2 does not show such behavior.

3.2 Viscous flows

Shock Wave/Boundary Layer Interaction. This test case is with a two-dimensional laminar flow, characterized by an oblique shock with an incident angle of $32.585°$ upon a flat plate causing a boundary layer to separate and reattach around the shock-impinging region. The complicated phenomenon provides a good test of validating a scheme before a turbulence model is implemented. The free stream conditions are as follows:

- Calorically perfect gas
- $M_\infty = 2.0$
- $Re = 2.96\times10^5$
- Pr=0.72
- $\theta_{impinging} = 32.585°$

The conditions for the computations are as follows:

- Spatial discretization :
  Roe's FDS, RoeM 1, RoeM 2 and HLLE
  2nd order accuracy with van Leer's limiter
  Number of grid points = 105×65
- Boundary condition :
  Adiabatic wall condition

Figure 10 shows pressure contour of each scheme. Impinging shock wave and circulatory flow where flow is separated and reattached are well resolved. No spurious oscillation near oblique shock and wall is observed. In Fig. 11, skin friction coefficients of RoeM 1 and RoeM 2 are compared with the results of Roe's FDS and the experimental data of Ref. [11]. Figure 11 shows that skin friction coefficients of all the proposed schemes are in very good agreement with those of Roe's FDS and experimental data, indicating the capability of all the proposed schemes to compute viscous flows involving shock waves and flow separation. The error histories of the proposed schemes show similar convergent rates to Roe's FDS.

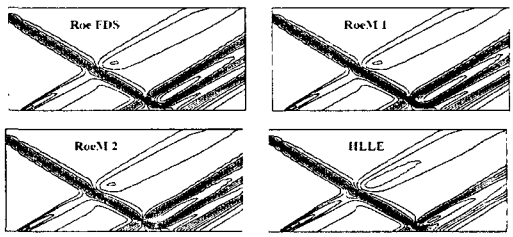

Fig. 10. Pressure contour

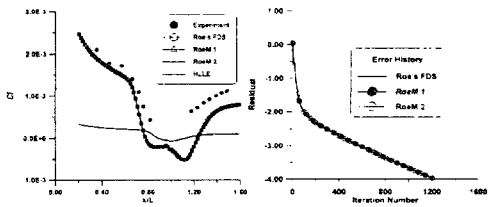

Fig. 11. Skin friction coefficient and error history

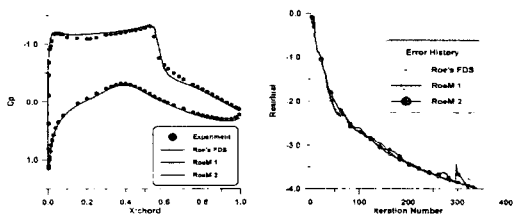

Fig. 12. Cp distribution and error history

Transonic Flow around RAE2822 Airfoil. This test case is concerned with viscous turbulent flow around RAE2822 airfoil at the

transonic flow regime. The free stream conditions are as follows:

- Calorically perfect gas
- $M_\infty = 0.73$
- $Re = 6.5 \times 10^6$
- Pr = 0.72
- $\alpha = 2.79^\circ$

The conditions for the computations are as follows:

- Spatial discretization :
  Roe's FDS, RoeM 1, RoeM 2
  2nd-order accuracy with van Leer's limiter
  241×48 C-type mesh
- Boundary condition :
  No-slip adiabatic wall condition

The conditions correspond to the experimental Case 9 in Ref. [12]. The Baldwin-Lomax turbulence model is used. The flow is assumed to be fully turbulent without any transition near the leading edge. Figure 12 shows Cp distributions and error history. Differences between the current schemes and Roe's FDS are hardly noticeable. This results show a fairly accurate Cp distribution compared with the experimental data.

Hypersonic Flow around a Blunt Body. As a final test case, a hypersonic blunt body problem is chosen in order to examine the effects of a strong shock discontinuity and large gradients in a boundary layer. In computing this problem, the primary concern is the accurate prediction of the surface heating rate at the wall. The free stream conditions are as follows:

- Calorically perfect gas
- $M_\infty = 16.32$
- $p_\infty = 82.95 (N/m^2)$
- $\rho_\infty = 5.557 \times 10^{-3} (kg/m^3)$
- $\mu_\infty = 3.369 \times 10^{-6} (kg/m \cdot s^2)$
- $T_\infty = 52K$
- $T_{wall} = 294.4K$
- $Re = 1.4972 \times 10^5$
- Pr = 0.72

The conditions for the computations are as follows:

- Spatial discretization :
  RoeM 1 and RoeM 2
  3rd-order accuracy with minmod limiter
  Number of grid points = 65×113
- Boundary condition :
  Constant temperature wall

Roe's FDS is not used for this test due to the shock instability, i.e. the carbuncle phenomenon. We just compare the numerical results with the experimental data.[13] Figure 13 shows surface heating rates of all the proposed schemes, indicating a very good agreement with the experimental data.

4. Conclusions

From Roe's FDS, the linearized Riemann-solver, Roe with Mach number-based function (RoeM) schemes that are free from the shock instability are developed. In order to control pressure contribution in the mass flux, which is considered to be the source of the shock instability,

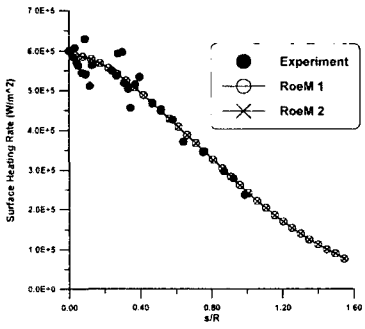

Fig. 13 Surface heating rate

a control function f is introduced. The function f has the role of reducing the rate at which pressure perturbation feeds the density field. The function

g that is used in RoeM 2 has the role of increasing the rate at which density perturbation is damped out. New wave speed is introduced to remedy expansion shock and instability in the expansion region, while still preserving the capability to capture contact discontinuity exactly. For the accurate prediction of the surface heat transfer rate, RoeM schemes are designed to preserve total enthalpy. Although control function f and g are very simple and other better formulations may exist, numerous computational tests performed in this paper show that the proposed schemes are able to solve a wide range of aerodynamic problems, accurately and without the shock instability, especially where strong shock wave exists.

Acknowledgements

The authors appreciate the financial support by Agency for Defense Development (ADD) and by the Brain Korea-21 Program for the Mechanical and Aerospace Engineering Research at Seoul National University.

References

[1] Godunov, S. K., 1959, "A difference scheme for the numerical computation of discontinuous solutions of hydrodynamic equations," Math. Sbornik, Vol. 47, p. 271

[2] Roe, P. L., 1981, "Approximate Riemann solver, parameter vectors, and difference scheme," *J. of Computational Physics,* Vol.43, p. 357

[3] Osher, S. and Chakravarthy, S., 1983, "Upwind scheme and boundary conditions with applications to Euler equations in generalized geometries," *J. of Computational Physics,* Vol. 50, p. 447

[4] Einfeldt, B., Munz, C. D., Roe, P. L and Sjögreen, B., 1991, "On Godunov-type methods near low densities," *J. of Computational Physics,* Vol. 92, p. 273

[5] Peery, K. M. and Imlay, S. T., 1988, "Blunt-body flow simulations," AIAA Paper 88-2904

[6] Quirk, J. J., 1994, "A contribution to the great Riemann solver debate," *Int. J. for Numerical Methods in Fluids,* Vol. 18, p. 555

[7] Wada, Y. and Liou, M. S., 1997, "An accurate and robust flux splitting scheme for shock and contact discontinuities," *SIAM J. Sci. Comput.,* Vol. 18, p. 633

[8] Lin, H. C., 1995, "Dissipation addition to flux-difference splitting," *J. of Computational Physics,* Vol. 117 p. 20

[9] Liou, M. S., 2000, "Mass flux schemes and connection to shock instability," *J. of Computational Physics,* Vol. 160, p. 623

[10] Gressier, J., Moschetta, J. M., 2000, "Robustness versus accuracy in shock-wave computations," *Int. J. Numer. Meth. Fluids.* Vol. 33, p. 313

[11] Hakkinen, R. J., Greber, I., Trilling, L. and Abarnel, S. S., 1957, "The interaction of an oblique shock wave with a laminar boundary layer," Tr 57-1, Fluid Dynamics Research Group, MIT

[12] Cook, P. H., McDonald, M. A. and Firmin, M. C., 1979, "Airfoil RAE 2822 pressure distributions, boundary layer and wake measurements," AGARD Advisory Report 138

[13] Holden, M. S., Weiting, A. R., Moselle, J. R. and Glass, C., 1988, "Studies of aerothermal loads generated in regions of shock/shock interaction in hypersonic flow," AIAA Paper 88-0047